Open Research Online
The Open University's repository of research publications
and other research outputs

OpenMARS: A global record of martian weather from 1999 2015

Journal Item

oro.open.ac.uk

OpenMARS: A global record of martian weather from 1999 2015

James A. Holmes [a],[*], Stephen R. Lewis [a], Manish R. Patel [a],[b]

[a] School of Physical Sciences, The Open University, Milton Keynes, MK7 6AA, UK
[b] Space Science and Technology Department, Science and Technology Facilities Council, Rutherford Appleton Laboratory, Harwell Campus, Didcot, Oxfordshire, OX11 0QX, UK

ARTICLE INFO

ABSTRACT

The Open access to Mars Assimilated Remote Soundings (OpenMARS) dataset is a reanalysis product combining past spacecraft observations with a Mars Global Circulation Model (GCM). The OpenMARS product is a global surface/atmosphere reference database of surface and atmospheric properties for almost nine Mars years that can be used by Mars scientists and engineers interested in global surface/atmospheric conditions and the physical, dynamical and chemical behaviour of the atmosphere for the recent past on Mars.

In the OpenMARS dataset, spacecraft observations of temperature, dust and water vapour from the Thermal Emission Spectrometer (TES) instrument on the NASA Mars Global Surveyor spacecraft, temperature and dust from the Mars Climate Sounder (MCS) instrument aboard NASA's Mars Reconnaissance Orbiter spacecraft and ozone from the Spectrometer for the Investigation of the Characteristics of the Atmosphere of Mars (SPICAM) instrument on the European Space Agency (ESA) Mars Express orbiter are combined with a Mars GCM used at the Open University.

1. Introduction

A reference dataset for the martian atmosphere and surface that provides the best estimate of the past weather on Mars has for a long time been sought by scientists and engineers looking to send satellites to orbit Mars and for landing rovers and surface platforms on the surface, resulting in the creation of the Mars Climate Database (Lewis et al., 1999), perhaps the most prevalent reference dataset used so far. While it has been extensively validated with current observations, it does not combine output from the Mars global circulation model (GCM) with current and past retrievals; a process which is commonplace on Earth in particular for forecasting the global weather and providing the best dataset of the past climate (Dee et al., 2011). A synergism of retrievals of the atmosphere of Mars with one of the world's leading Mars global circulation models is a key next step towards this goal in providing accurate forecasting and reanalyses akin to what we have available to us on Earth.

To address some of the limitations noted above, we have created the Open access to Mars Assimilated Remote Soundings (OpenMARS) dataset to be used as a reference dataset of the actual global weather occurring on Mars from 1999 to 2015. This dataset is able to sit alongside the MCD dataset that provides a smoothed seasonal climatology for varying dust scenarios. While the MCD datset provides multiple different scenarios that can be used to explore the parameter space of key variables of high importance to landing a rover on Mars (for example), the OpenMARS dataset provides the best estimate of the atmospheric state for the past 9 Mars years, with the global state of the atmosphere constrained by observational datasets and physical laws in the Mars GCM (in particular for spatio-temporal regions for which observations are not available nearby). The OpenMARS dataset would therefore be more appropriate to use as the best estimate of the atmospheric state when re-processing past satellite observations of the martian atmosphere, or for investigating specific past weather events that have occurred on Mars from 1999 to 2015. The OpenMARS dataset however does not contain simulations of the thermosphere, or several trace gases (such as CO and odd hydrogen species) that are present in the martian atmosphere, so it would be more appropriate to use the MCD for these investigations. If the user would also prefer to look at a wider parameter space of atmospheric dust content, for quick and easy estimates of potential extreme conditions upon atmospheric entry of a spacecraft as an example, the MCD would be more appropriate than the OpenMARS reanalysis dataset.

Two other reanalyses products for the Mars atmosphere have previously been created to this date. The Ensemble Mars Atmosphere Reanalysis System (EMARS) is fully described in Greybush et al. (2012), and
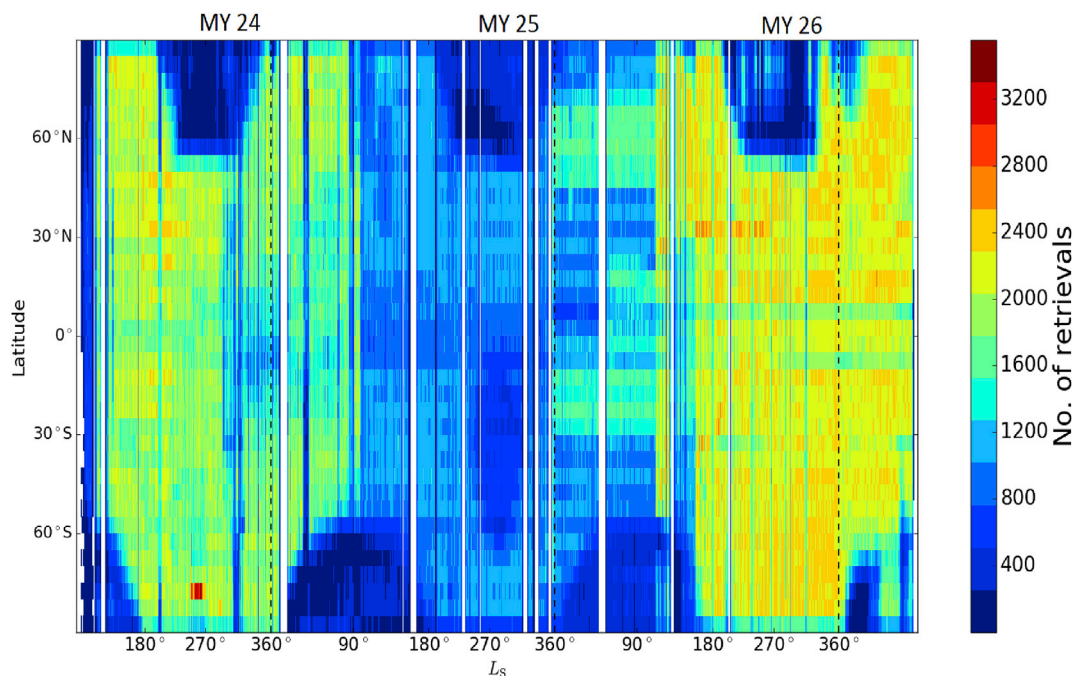
Fig. 1. Number of TES temperature profiles after quality control in 2 sol by 5° latitude bins. Dashed vertical lines indicate the end of a Mars year. White indicates no data available in this particular bin.

has recently been made publicly available (Greybush et al., 2019a,b). In the EMARS reanalysis product, retrievals of Thermal Emission Spectrometer (TES) and Mars Climate Sounder (MCS) temperature profiles are assimilated into the Geophysical Fluid Dynamics Laboratory Mars GCM (Greybush et al., 2019a,b) that includes a finite volume dynamical core based on a longitude-latitude coordinate system. The EMARS reanalysis uses the Local Ensemble Transform Kalman Filter assimilation scheme (Hunt et al., 2007) to assimilate the temperature profiles, with fundamental surface and atmospheric variables output on a 5° latitude by 6° longitude grid and on 28 vertical levels up to around 90 km.

A second reanalysis, the Mars Analysis Correction Data Assimilation (MACDA) dataset has been created and detailed by Montabone et al. (2014) using a past version of the same Mars GCM used to create the OpenMARS reanalysis product. The MACDA dataset is a reanalysis of TES temperature profiles and TES dust column optical depth retrievals over almost three Mars years. The data are publicly available from the National Centre for Atmospheric Science British Atmospheric Data Centre, with the aim of fostering scientific analyses and to allow applications of the long-term martian dust climatology, and contain two-hourly output of fundamental atmospheric and surface variables on a 5° longitude-latitude grid extending on 25 vertical levels from the surface to an altitude of around 100 km.

For times at which observational data are available (and over a defined time window around each observation), the Analysis Correction (AC) data assimilation scheme (Lorenc et al., 1991) is used to update the temperature and column dust optical depth fields (using TES temperature profiles and column dust optical depth retrievals respectively). In the case of assimilation of TES temperature profiles, the assimilation scheme also updates the wind fields to ensure that any changes balance the thermal data input into the GCM. In the case of local column dust optical depth, when no further retrievals are available for assimilation, the column dust optical depth remains fixed until further retrievals are assimilated into the GCM.

The MACDA reanalysis dataset has been used to study multiple different topics related to Mars, including transient eddies (Mooring and Wilson, 2015), energetics of the martian atmosphere (Battalio et al., 2016) and the structure of the polar vortices (Waugh et al., 2016) which also includes a comparison of the EMARS and MACDA reanalysis

products. There are, however, a few limitations of the MACDA reanalysis. The dust particles in the GCM were prescribed in both the horizontal and vertical dimensions and therefore not transported. The EMARS reanalysis allowed for the vertical transport of dust particles with the horizontal distribution constrained by observations (Montabone et al., 2015). The vertical distribution of the dust is analytically prescribed in the MACDA dataset using a modified form of the Conrath distribution (Conrath, 1975), which following the discoveries of detached dust layers (Heavens et al., 2014) is less valid than previously thought. Observational data are also available for later Mars years from more recent spacecraft, such as the Mars Reconnaissance Orbiter (MRO). For any statistical studies using the MACDA dataset a longer time series would be preferable, and assimilation of additional observational datasets to extend the timescale covered by the MACDA reanalysis would provide a more robust reanalysis product. The above limitations are some of the more pertinent reasons for the creation of the OpenMARS dataset.

In this paper, we detail the OpenMARS reanalysis product, a dataset containing directly assimilated temperature, dust opacity, water vapour column and ozone column from multiple observational datasets. Section 2 gives an overview of the observational data, the Mars GCM and the data assimilation scheme used to create the OpenMARS reanalysis product and section 3 displays an overview of the output contained in the OpenMARS reanalysis product. Section 4 describes a comparison of the OpenMARS reanalysis product to assimilated observations, while section 5 details the format of the OpenMARS reanalysis data files. Finally, section 6 describes how an interested user can access the OpenMARS reanalysis product.

2. Components of the OpenMARS dataset

To create the OpenMARS dataset observations of the martian atmosphere from several different instruments on multiple orbiters have been combined with a Mars GCM using the AC data assimilation scheme. These three components are now detailed in the following sections.

2.1. Observational data

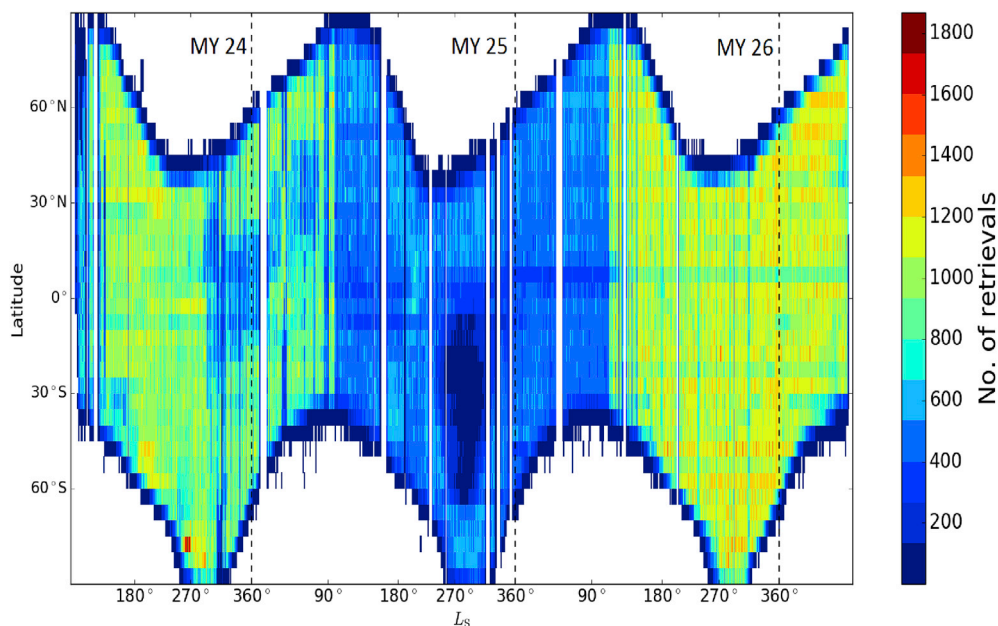The following section describes the observational datasets that have

Fig. 2. Number of TES dust opacity retrievals after quality control in 2 sol by 5° latitude bins. Dashed vertical lines indicate the end of a Mars year. White indicates no data available in this particular bin.

been assimilated to create the OpenMARS dataset, which cover almost 9 Mars years of observation and provide the largest spatio-temporal reanalysis dataset for the martian atmosphere.

2.1.1. TES data

The Thermal Emission Spectrometer (TES) instrument, aboard the Mars Global Surveyor (MGS) spacecraft operates in the thermal infrared between 6 and 50 μm (200–1600 cm^{-1}). The spectrometer began its mapping operations on March 1, 1999 ($L_S = 104°$, MY 24) and ended on August 31, 2004 ($L_S = 81°$, MY 27). MGS completed 12 orbits each sol, creating two sets of 12 narrow strips of data, running roughly north-south and separated by around 30° in longitude. The two sets of data contain observations at local times around 2 a.m. and 2 p.m. respectively, with the variation larger near the poles (for example, in the polar regions the daytime observations range between 12:30–14:30).

The temperature retrievals used in the assimilation, along with the retrieval methods, are described in detail by Smith et al. (2000) and Smith (2004). Temperature profiles are retrieved from nadir radiances in the 15 μm CO_2 band, and extend up to an altitude of around 40 km. The vertical resolution is around one pressure scale height (around 10 km), though the temperature retrievals provided for assimilation have a vertical sampling on a one-quarter pressure scale height (around 2.5 km). Uncertainties for each profile are around 2 K, but are larger in the lowest scale height above the ground because of possible errors in estimating the surface pressure (Conrath et al., 2000; Smith, 2004). While systematic errors are present for each retrieval, they peak with values greater than 5 K in retrievals over the winter polar regions because the absolute radiometric calibration affects the retrievals most strongly under cold atmospheric and surface conditions (Conrath et al., 2000). Evidence for systematic errors was found in retrievals with temperatures lower than the CO_2 condensation temperature: it would be expected that the latent heat released during condensation would keep the temperature close to the CO_2 condensation temperature of around 145 K. Fig. 1 displays the number of TES temperature profiles that are assimilated to form part of the OpenMARS reanalysis product. Throughout its lifetime, the TES instrument retrieved approximately 46 million temperature profiles. Fewer temperature profiles are available during the majority of MY 25 as the TES instrument during this period was observing at a higher spectral resolution that took twice as long to acquire compared to running at the

lower resolution for the rest of the time period covered by the observations.

The TES instrument in nadir-viewing geometry measured dust opacity at 1075 cm^{-1} in the infrared, with the retrievals method detailed in Smith et al. (2000). Using the TES spectra, an equivalent column-integrated opacity of pure absorbers as a function of wavenumber is first computed. Then, the contribution of dust to the total opacity is estimated by fitting predetermined spectral shapes (opacity as a function of wavenumber) for dust, water ice, and the effect of a non-unit emissivity surface to the observed opacity spectrum. Fig. 2 displays the number of TES column dust optical depth retrievals that are assimilated to form part of the OpenMARS reanalysis product. Over the time period used for the present reanalysis, around 16 million TES dust opacity retrievals are available for assimilation. There is a notable lack of coverage of column dust optical depth retrievals at high latitudes during polar winter of each Mars years, a result of the minimal thermal contrast between the surface and atmosphere preventing a reliable retrieval being derived. Fewer retrievals of column dust optical depth are also available during the majority of MY 25 for the exact same reason detailed in the description of the TES temperature profiles, namely that the TES instrument during this time was observing at a higher spectral resolution.

The quality control applied to the TES temperature profiles follows the procedure described in Lewis et al. (2007). Profiles marked as bad by the retrieval algorithm are automatically rejected, with remaining retrievals filtered to remove any profiles that fall significantly below the CO_2 saturation curve in a similar method to Montabone et al. (2014). This additional filtering is applied in order to remove excessively high or low temperatures which may cause problems with the model's physical schemes, and also removes some of the retrievals affected by possible systematic errors in the radiometric calibration. The filtering removes around 0.5% of the available observations.

For dust opacity, the quality control procedure is also detailed fully in Lewis et al. (2007). Following Smith et al. (2000), only opacities where the surface temperature was greater than 220 K were retained. This requirement, for a good surface-atmosphere temperature contrast, unfortunately further restricts the dust information to daytime. Most dust information is in the equatorial region and the southern hemisphere. Finally, checks were run to see that the dust opacity and the
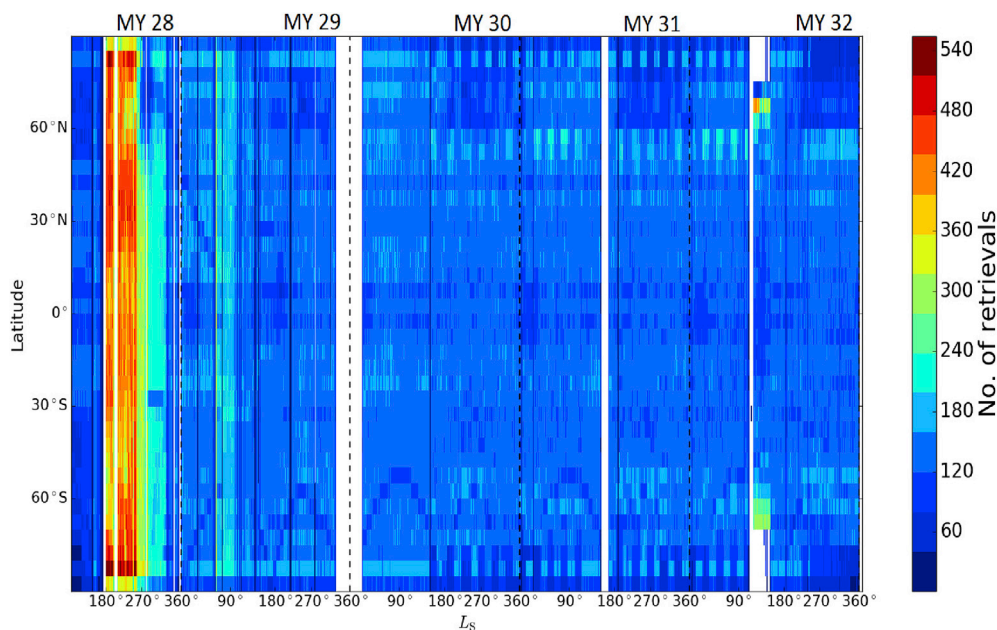
Fig. 3. Number of MCS temperature profiles after quality control in 2 sol by 5° latitude bins. Dashed vertical lines indicate the end of a Mars year. White indicates no data available in this particular bin.

simultaneously retrieved water ice opacity were both positive and that the total fit residual was not too large (Lewis et al., 2007).

2.1.2. MCS data

The Mars Climate Sounder (MCS) instrument, aboard the MRO spacecraft, employs a nearly continuous limb viewing strategy in order to achieve greatly increased sensitivity to minor and trace constituents (McCleese et al., 2007). The instrument is a passive radiometer which retrieves in 9 spectral bands covering the visible and mid-to far-infrared channels. It is capable of retrieving vertical profiles of water ice and dust opacity alongside temperature profiles with a greater vertical resolution than TES (5 km for MCS as opposed to around 10 km for TES). The vertical coverage of the profiles is from the surface up to altitudes of

around 85 km (as opposed to around 40 km for TES). The MCS observations comprise two sets of twelve narrow strips of data, separated by around 30° in longitude, a similar pattern to that observed by the TES instrument, with only along-track MCS profiles currently included. Due to the Sun-synchronous orbit of MRO, the MCS observations away from the pole occur at local times around 3 a.m. and 3 p.m. though the actual local time of an observation varies with both latitude and season. The instrument began its coverage of Mars on September 24, 2006 (or $L_S = 111°$ MY 28), in the primary science phase of the mission.

The retrieval of vertical temperature profiles from the MCS measured radiance is extensively covered in Kleinböhl et al. (2009) and briefly detailed in this section. MCS retrievals from version v4.3 are used for the current version of the OpenMARS reanalysis product. It uses 3 channels
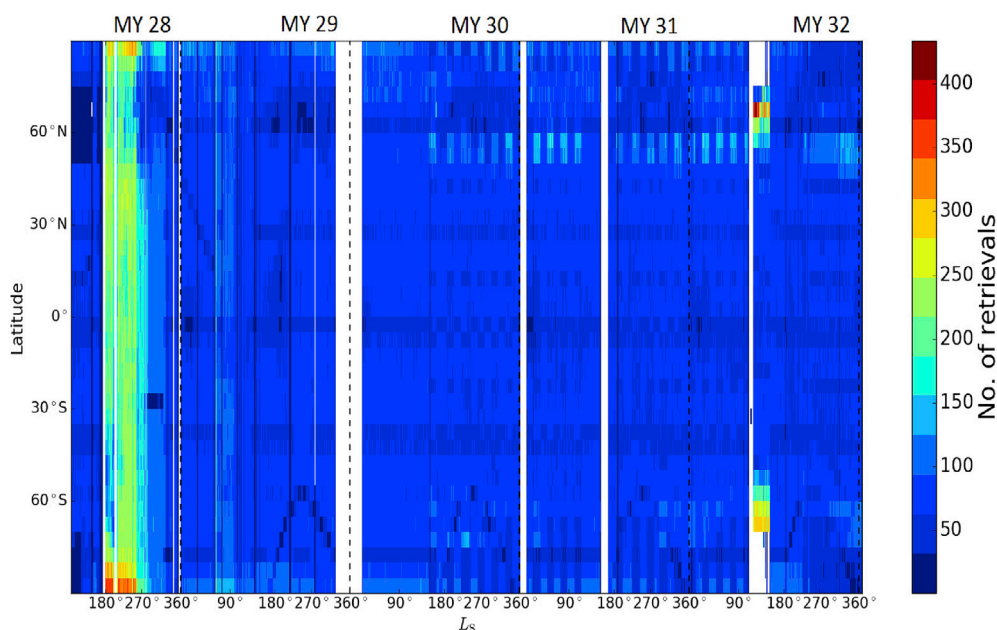

Fig. 4. Number of MCS dust opacity retrievals after quality control in 2 sol by 5° latitude bins. Dashed vertical lines indicate the end of a Mars year. White indicates no data available in this particular bin.

of the MCS instrument (A1-3) in the far-infrared. The radiative transfer equation is inverted to determine the temperature from the radiance using an iterative method. For this process, a 'first guess' is needed for the temperature profile, although the success of this retrieval method is shown to be insensitive to this initial guess (Kleinböhl et al., 2009). The algorithm is processed for each limb profile with 30 iterations, to converge on the final vertical profile of temperature. The error on the retrieval is reduced in the lower atmosphere (0.5 K) and increases at higher altitudes due to the reduction in signal-to-noise ratio (> 1 K above 40 km) and in situations where the atmosphere is opaque.

Fig. 3 displays the number of MCS temperature profiles that are assimilated to form part of the OpenMARS reanalysis product. After quality control, around 7.5 million temperature profiles retrieved by the MCS instrument are assimilated. An increased number of MCS temperature profiles are noticeable at the end of MY 28, as a result of a dedicated campaign to observe as much as possible of the martian atmosphere during a high dust loading dust storm season. Periods in which there are no data at all (e.g. at the end of MY 29) are as a result of the MCS instrument being switched off during this time period.

The retrieval of dust opacity profiles from the MCS measured radiance is also extensively covered in Kleinböhl et al. (2009). Details of how the column dust optical depth is retrieved are presented in Montabone et al. (2015) and briefly detailed here. For any given successful limb retrieval, the full profile of dust extinction opacity produced by the retrieval algorithm (MCS retrievals from version v4.3 are used for the current version of the OpenMARS reanalysis product) is integrated to produce a column dust optical depth. The profile is extended upward and downward under the assumption of well mixed dust, based on the last valid value. The MCS dust profiles cannot be retrieved down to the surface using only limb observations, and the dust in the un-retrieved part of the profile can potentially account for a significant fraction of the total dust column. Therefore estimates of column dust optical depth from MCS observations have the possibility of errors attributable to either the extrapolation to the surface under the well mixed assumption or the use of dust opacity values at altitudes where the fit to observed radiances is not within the standard threshold. The well mixed assumption in particular is less valid with the discovery of detached dust layers found in MCS profiles (Heavens et al., 2014).

Fig. 4 displays the number of MCS column dust optical depth retrievals that are assimilated to form part of the OpenMARS reanalysis product. During the time period covered by the MCS instrument, around 4 million column dust optical depth retrievals are assimilated. The retrieval method allows for a reliable measurement of dust optical depth during the daytime and nighttime during polar winter over this time period. As with the MCS temperature profiles, more retrievals are available at the end of MY 28 as a result of the dedicated campaign to observe as much as possible during the high dust loading dust storm season.

The quality control applied to the MCS temperature profiles is described in Lewis et al. (2007) and is precisely the same process as is described for the TES temperature profiles in the previous section. Quality control for the derived MCS column dust optical depth retrievals is fully described in Montabone et al. (2015) and briefly detailed here. Estimates of the MCS column dust optical depth can be fairly inaccurate if the lowest retrieved level of dust opacity is above around 20 km altitude, depending on the time of the year and the dust/water ice conditions. The dataset therefore largely consists of nighttime retrievals that correspond to dust extinction profiles with valid values at or below 25 km altitude, and only retrievals with local times between 12 p.m. and 6 p.m. when the corresponding extinction profile has valid values at or below 8 km altitude are accepted. Finally, estimates of column dust optical depth where the temperature profile dropped below the condensation temperature of carbon dioxide at some of the pressure levels are rejected, because CO_2 ice opacity is currently not taken into account in the retrieval algorithm but can affect retrievals of dust opacity at those levels.
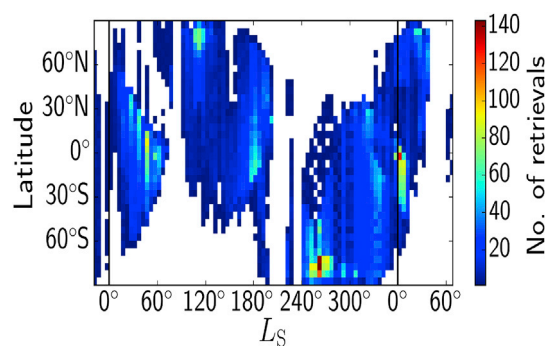

Fig. 5. Number of retrievals of SPICAM total ozone abundance after quality control in $5°L_S$ by $5°$ latitude bins for the whole of MY 27 and the end/beginning of MY 26/MY 28. Solid vertical lines indicate the end of a Mars year. White indicates no data available in this particular bin.

2.1.3. SPICAM total ozone data

The Spectrometer for the Investigation of the Characteristics of the Atmosphere of Mars (SPICAM) instrument, aboard the Mars Express (MEx) spacecraft, is comprised of a dual UV/IR spectrometer. In the UV spectral range, it observed from 115 to 310 nm and is capable of ozone column density retrievals due to the strong Hartley band of ozone absorption around 250 nm. SPICAM was the first orbiting instrument capable of providing a global total ozone climatology with decent spatial and temporal coverage (Perrier et al., 2006).

The retrieval of total ozone from the Hartley band of intense absorption (220–280 nm) is described fully in Perrier et al. (2006). The outcome of the retrieval process is just over 27,000 high signal-to-noise ratio observations for almost one and a half martian years ($L_S = 341°$ in MY 26 to $L_S = 121°$ in MY 28). The binned number of retrievals from SPICAM is shown in Fig. 5. The algorithm to retrieve the ozone column from the solar backscattered UV radiation in this version is a relative method, with the measured spectra divided by a reference spectrum, taken to be over Olympus Mons. This location is used since it is a region known to have extremely low ozone density values and minimal dust and aerosols in the atmospheric column owing to the low surface pressure and total column mass. The division by the reference spectrum filters out instrumental effects.

A forward radiative transfer model, containing assumptions on surface pressure, vertical ozone profile and temperature, is computed taking into account the geometry of the considered observation. The vertical distribution of dust follows the Conrath profile (Conrath, 1975) which was analytically derived from considerations of particle sedimentation and eddy mixing to vary the height that dust can reach in the atmosphere at different times of a Mars year. The a priori information is taken from the Laboratoire de Météorologie Dynamique (LMD) GCM, with a two-step method used to perform the retrieval. The model first computes the spectra assuming a dust-free atmosphere, and then in the second step the modelled spectra are adjusted to the observed spectra by least square minimisation to retrieve the ozone column density, surface albedo and dust opacity, which are the three free parameters. To remove observations which have a low signal-to-noise ratio, observations with a solar zenith angle less than 85° and emission angle less than 30° are rejected. The relative method used does not currently take into account the effect of clouds, although any biases introduced due to the neglect of clouds has been investigated previously by Perrier et al. (2006). Using synthetic realistic spectra and the forward model, they found the retrieval error increased to almost 100% with high cloud opacity (cloud opacity greater than 1) but this occurs infrequently on Mars and primarily in polar winter regions where there are no SPICAM retrievals. An average error of 10–15% in total ozone was calculated for much more common thinner clouds (cloud optical depth between 0.1 and 0.2). The ground resolution of the SPICAM observations at pericentre is around 4 km^2.
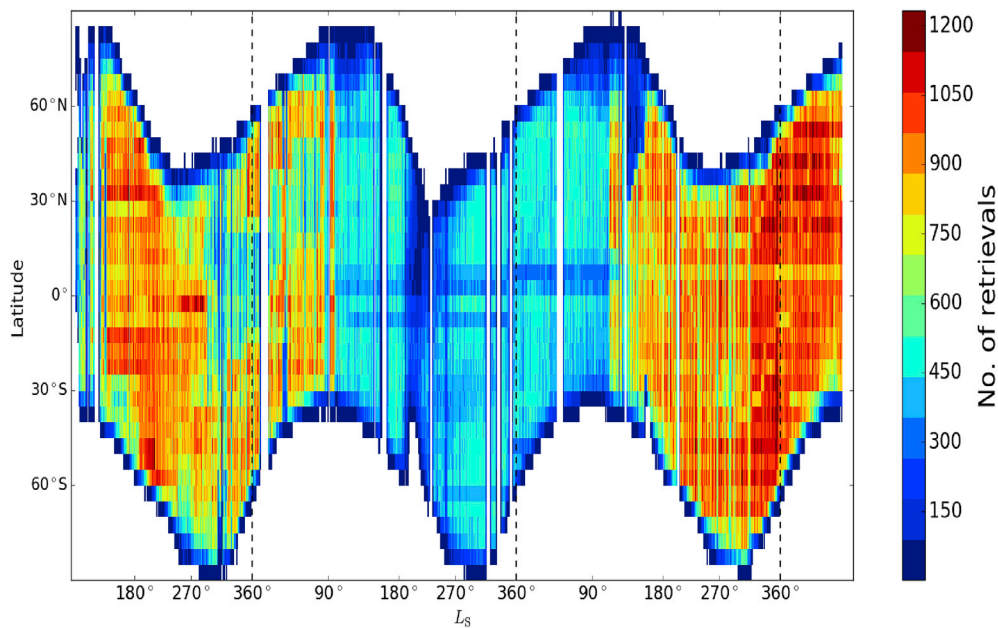
Fig. 6. Number of retrievals of TES water vapour column after quality control in 2 sol by 5° latitude bins. Dashed vertical lines indicate the end of a Mars year. White indicates no data available in this particular bin.

Before the SPICAM retrievals are assimilated to create part of the OpenMARS reanalysis product, they are subject to further quality control measures which are detailed in Holmes et al. (2018). For the almost 27,000 retrievals from SPICAM available, each individual SPICAM retrieval R_i is compared to the retrieval $R_{i\pm1}$ either side of it in time. Spurious retrievals are then flagged up using three criteria; $| R_i - R_{i\pm1} | > 10$ μm-atm, $| L_i - L_{i\pm1} | < 5°$ and $| S_i - S_{i\pm1} | < 1$ where L_i and S_i are the latitude and sol of observation i respectively. A value of 10 μm-atm was chosen to avoid rejection of retrievals which are realistic due to the sharp gradient on the boundaries of the high polar ozone abundance. This quality control method removes only 7 retrievals from the dataset.

2.1.4. TES water vapour column data

The only water vapour column data currently publicly available for assimilation into the OpenMARS reanalysis product are from the TES instrument aboard the MGS spacecraft, described in Section 2.1.1. Water vapour column retrievals are obtained by comparing synthetic spectra with TES spectra from rotation bands in the 28–42 μm region. In this region, the TES signal-to-noise ratio is relatively high, and the contribution to the spectrum from water vapour can easily be separated from the dust, water ice and surface contributions (Smith, 2002). When calculating the synthetic spectra, water vapour is assumed to be well mixed up to the condensation level, and zero above. The estimated uncertainties in the vapour column abundance caused by random errors are 3–5 pr-μm, while uncertainty in the pressure broadening of water vapour by CO_2 results in a systematic error likely to be much less than 25%.

Full details of the quality control are in Steele et al. (2014b). Because of the restrictions of the retrieval algorithm, water vapour retrievals are only provided for locations where the surface temperature is greater than 220 K, which excludes data from the nighttime orbits and over the winter polar regions. The number of TES retrievals varies with time, but in full operational mode each strip of data typically contains around 700 retrievals, spaced around 0.15° (10 km) apart in latitude. The TES instrument retrieved approximately 13 million water vapour columns during its lifetime, with the number of retrievals binned into discrete latitude-time periods shown in Fig. 6, although the OpenMARS reanalysis product currently only includes retrievals from $L_S = 173°$ MY 24 to $L_S = 186°$ MY 25.

For the vapour column observations, the variation with latitude can be quite large due to differences in topography and temperature, but nearby measurements should conform to within a specified threshold. To investigate possible spurious observations, a buddy-check was applied on each strip of data after all retrievals had been scaled to the 610 Pa pressure level to remove the effects of topography. For each observation, the buddy-check compares the value to the mean of all the observations within a specified meridional distance d either side of it. The observation is highlighted as a possible error if its value differs by some threshold value δ_{vap}. As the vapour column is strongly dependent on latitude, applying a buddy-check with large values of d removes observations with natural variation. Conversely, small values of d results in too few observations to perform a meaningful statistical analysis. Numerous tests showed that comparing observations over a distance d = 300 km (around 5° in latitude), and excluding any observations where $\delta_{vap} > 3\sigma$ (around 4–10 pr-μm depending on location and season) from the mean, gave the best combination of a large enough sample of data for comparison, the removal of spurious observations and the retention of observations with natural variation. Only a small fraction of the water vapour column observations are discarded (around 0.5%) by the buddy-check algorithm and so it does not negatively impact on the amount of data available for assimilation into the OpenMARS reanalysis product.

2.2. Mars Global Circulation Model

The GCM used to create the OpenMARS reanalysis product is the UK version of the LMD GCM (hereafter MGCM), which has been developed in a collaboration of the Laboratoire de Météorologie Dynamique, the Open University, the University of Oxford and the Instituto de Astrofísica de Andalucía. This model uses physical parameterisations shared with the LMD GCM, which are coupled to a UK-only spectral dynamical core alongside an energy and angular momentum conserving vertical finite-difference scheme. Tracers such as CO_2, water vapour and dust are transported by a UK-only semi-Lagrangian advection scheme (Newman et al., 2002) with mass conservation (Priestley, 1993).

The MGCM used to create the OpenMARS reanalysis product is similar to the model used in Montabone et al. (2014) for a previous reanalysis dataset but the MGCM used for the OpenMARS reanalysis product includes additional sub-models. CO_2 is now transported as an
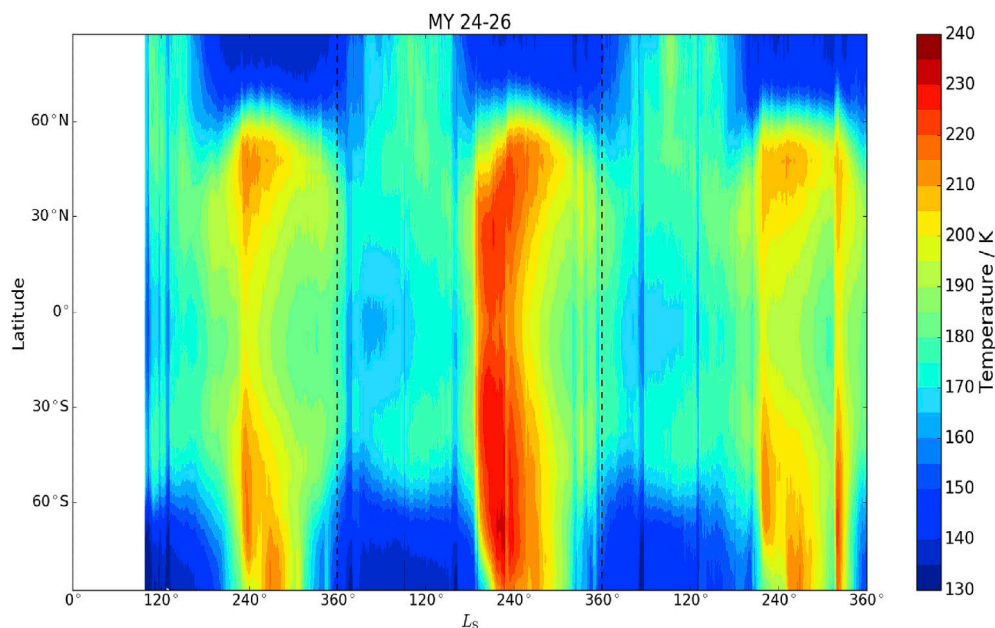
Fig. 7. Zonal-mean atmospheric temperature at 60 Pa and 3 p.m. local time in the OpenMARS reanalysis for MY 24 to MY 26. Dashed lines indicate the start of MY 25 and MY 26. White areas indicate no data.

additional tracer providing a better representation of the CO_2 cycle, with condensation and sublimation of carbon dioxide on the ground and in the atmosphere calculated from the local temperature and pressure state (Forget et al., 1998). A thermal plume model is used to better represent turbulent structures in the planetary boundary layer (Colaïtis et al., 2013), of importance for the evolution of tracers. A 'semi-interactive' two-moment scheme is used to freely transport dust in the model (Madeleine et al., 2011), although the dust column optical depth at each grid point is scaled to match the observed dust distribution from TES/MCS (depending on the time period covered) that is assimilated into the OpenMARS reanalysis product (Montabone et al., 2015). The MGCM is also coupled with the LMD photochemical module (Lefèvre et al., 2004, 2008) and uses a microphysical scheme for the water cycle (Navarro et al., 2014) to track and evolve 16 different chemical species in the atmosphere and on the surface including ozone and water vapour. Radiatively active clouds are not included, since previous modelling work has shown that it can introduce discrepancies as well as improvements to the temperature structure (Madeleine et al., 2012). The model is truncated at wavenumber 31 resulting in a 5° physical longitude-latitude grid (and 3.75° longitude-latitude grid for the dynamical core) with 35 vertical levels extending to an altitude of around 105 km. The time-stepping regime for the physical and dynamical parts of the MGCM is 15 and 1.5 min respectively.

2.3. Data assimilation scheme

To assimilate the observations and create the OpenMARS reanalysis product, the MGCM uses the AC scheme (Lorenc et al., 1991) with necessary parameters adapted to martian conditions. The AC scheme has previously been used to assimilate thermal and dust opacity retrievals from TES (Lewis and Barker, 2005) to indirectly study the thermal tides and also create the MACDA dataset (Montabone et al., 2014). The dust opacity retrievals have also been used to perform a multi-annual study of interannual dust variability (Montabone et al., 2005, 2015), indicating localised regions which triggered the onset of the global dust storm in MY 25 and also found dust lifting by dust devils to contribute little. Observations during the TES aerobraking phase have been assimilated indicating an atmospheric warming at the onset of

northern hemisphere winter due to the dust storm in MY 23 (Lewis et al., 2007). The AC scheme has also been validated against radio occultation (RO) measurements (Montabone et al., 2006), with the assimilation of TES thermal and dust opacity retrievals improving the agreement between the MGCM and the RO profiles. Recent work with the AC scheme has moved on to the assimilation of chemically passive water vapour and water ice (Steele et al., 2014b, a) to investigate the martian water cycle and radiative effect of water ice clouds respectively and chemically active species such as ozone (Holmes et al., 2018) and carbon monoxide (Holmes et al., 2019). The AC scheme is a form of successive corrections in which analysis steps are interleaved with each model dynamical time step. The modified successive corrections equation used by the scheme is

$$\mathbf{x}_a = \mathbf{x}_b + \mathbf{W}\tilde{\mathbf{Q}}(\mathbf{y}_o - H(\mathbf{x}_b)), \tag{1}$$

where $\mathbf{x}_a$ is the analysis vector, $\mathbf{x}_{ba}$ is the model background, $\mathbf{y}_o$ is the observation vector, H is the observation operator and $\mathbf{W} = \mathbf{BH}^T\mathbf{R}^{-1}$ and $\tilde{\mathbf{Q}}$ are matrices of weights and normalization factors respectively, with $\mathbf{B}$ the background error covariance matrix, $\mathbf{H}$ the linearization of the observation operator and $\mathbf{R}$ the sum of the observation and observation operator error covariance matrices. In each analysis step, the above equation is split into separate vertical and horizontal stages in order to spread the analysis increments from the observation locations to the surrounding model grid points. This is followed by the derivation of multi-variate increment fields for dynamical balance where applicable (e.g. after assimilating temperatures, balanced thermal wind increments are applied). Observations are inserted over an asymmetrical specified time window of 6 h (5 h before an observations valid time until 1 h after), optimally selected so that the assimilation will not unrealistically smooth out any inherent model variation. The asymmetrical time window is also used as it is beneficial because it biases the assimilation gains to regions ahead of the satellite ground track, which have not recently been observed. Spreading in time was also found to be beneficial in the case of relatively sparse data, where it is often better to use an observation from a slightly different time, with a reduced weight, rather than release the model which would then quickly relax back toward a temperature determined principally by its dust distribution, since the radiative timescale of the martian atmosphere is only 1–2 sols.
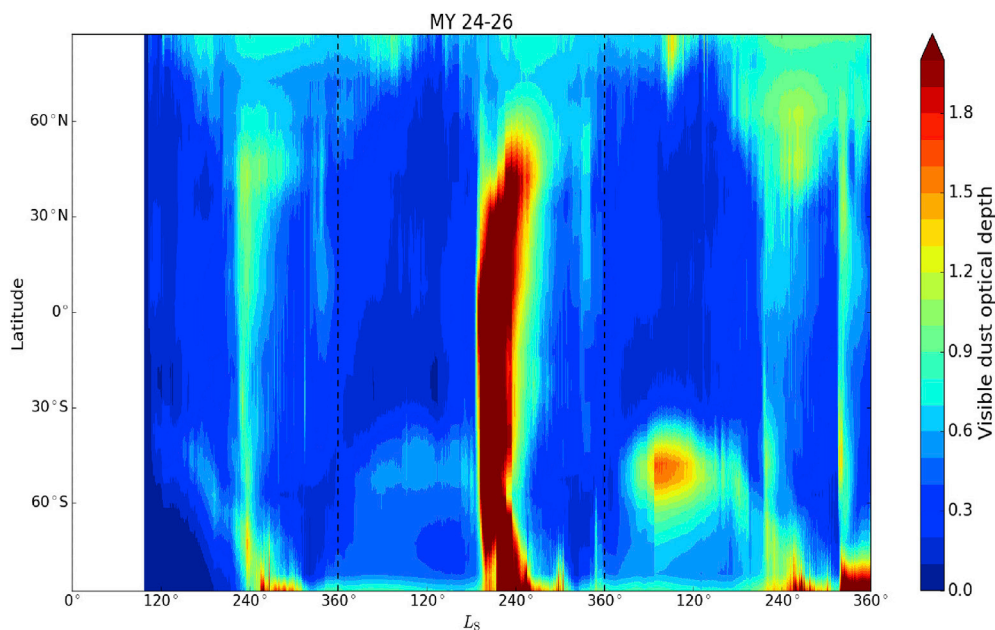
Fig. 8. Zonal-mean column dust optical depth (visible extinction at 0.67 μm) in the OpenMARS reanalysis for MY 24 to MY 26. Dashed lines indicate the start of MY 25 and MY 26. White areas indicate no data.

Temperature profiles from the TES and MCS instruments were assimilated into the OpenMARS reanalysis product using parameters which have previously been defined as optimal from numerous tests on the parameter space (Lewis et al., 1996, 1997, 2007). A normalised radius of influence for each observation equal to 3.5 correlation scales (equivalent to around 1200 km) is used for the temperature retrievals, consistent with previous assimilation of temperature profiles. This is equivalent to any temperature retrieval on the equator affecting the nearest four model grid points at its valid time with a weight dependent on the time factor and horizontal correlation scale (see Fig. 1 of Lewis et al. (2007)) and horizontal distance from the actual location of the retrieval assimilated.

Retrievals of column dust optical depth from the TES and MCS instruments were assimilated into the OpenMARS reanalysis with a slight alteration in parameters from those used for the MACDA reanalysis (Montabone et al., 2014). The normalised radius of influence for each observation is increased to 5 from 3.5 (used for MACDA) in an attempt to minimise the 'checkerboard' effect that can happen due to the spacing of the retrievals.

3. Sample output from the OpenMARS reanalysis product

The zonal-mean atmospheric temperature distribution at 60 Pa and 3 p.m. local time for the first three Mars years covered by the OpenMARS reanalysis product (i.e. covering the majority of the TES assimilation period) is shown in Fig. 7. Increased atmospheric heating of up to 15 K can be seen leading up to perihelion in MY 25 when compared to the
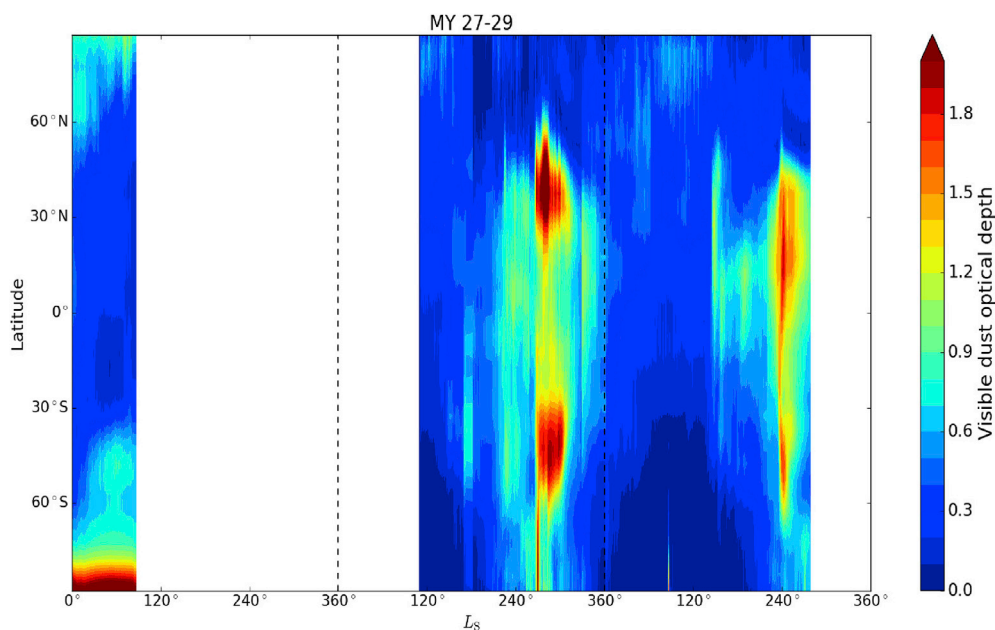

Fig. 9. Zonal-mean column dust optical depth (visible extinction at 0.67 μm) in the OpenMARS reanalysis for MY 27 to MY 29. Dashed lines indicate the start of MY 28 and MY 29. White areas indicate no data.
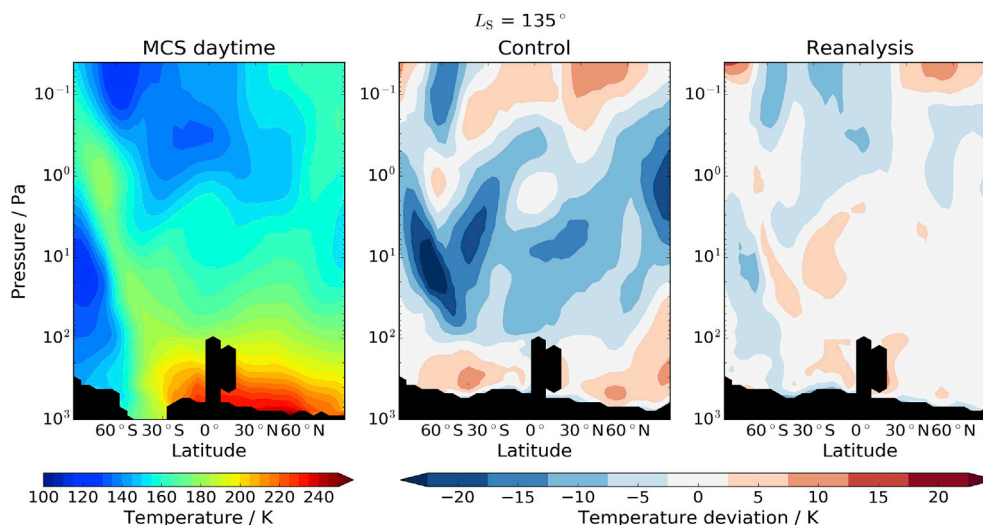
Fig. 10. Latitude-altitude plots of zonally and temporally averaged MCS daytime temperature retrievals (left), MCS–control temperature deviations (middle) and MCS–reanalysis temperature deviations (right). The temperature and temperature deviation are temporally averaged over a $30°$ L_S time period centred on $L_S = 135°$ MY 28. Black indicates regions of no data.

same time period in MY 24 and MY 26, corresponding to the global dust storm occurring in this Mars year.

The coldest atmospheric temperatures are seen in the polar winter of both hemispheres, with a clear distinction in mid-latitude temperature during the first and second half of each Mars year as a result of the increased atmospheric dust loading in the second half of the year and the elliptical orbit of Mars. Strips of decreased atmospheric temperature across all latitudes over particular time periods e.g. $L_S = 60$–$62°$ MY 26 are as a result of the lack of assimilated temperature retrievals over time periods of greater than 2 sols and short radiative timescale on Mars, with the OpenMARS reanalysis therefore reverting to the 'control' model state.

Fig. 8 displays the visible column dust optical depth covering the majority of the TES assimilation period. The observed absorption-only IR optical depth at 9.3 μm is converted to an IR extinction optical depth using a factor of 1.3 from Wolff and Clancy (2003), and then converted into a visible extinction optical depth at 0.67 μm using a factor of 2 from Madeleine et al. (2011). The global dust storm in MY 25 stands out with visible dust optical depths greater than 2. Levels of dust during the polar winter of both hemispheres seem initially to be quite varied from year to year, however in this region there are no TES column dust optical depth retrievals to assimilate (see Fig. 2). The assimilation process results in the last previous assimilated column dust optical depth being kept until updated by the next available retrievals in time, similar to the process used by MACDA (Montabone et al., 2014).

While no column dust optical depth retrievals were available in polar winter during the TES assimilation period, derivations of the column dust optical depth from vertical profiles of dust retrieved from the MCS instrument are available for later Mars years. The zonally averaged column dust optical depth for MY 27 to MY 29 is shown in Fig. 9. The observed MCS IR extinction optical depths are converted into an absorption-only IR optical depth at 9.3 μm using the method described in Montabone et al. (2015) without normalising onto a reference pressure level, and then converted into a visible extinction optical depth at 0.67 μm using a factor of 2 from Madeleine et al. (2011). In the polar winter of both hemispheres the visible column dust optical depth is reduced during the MCS period particularly when comparing with polar winter in MY 26 (see Fig. 8). Retrievals of column dust optical depth from the MCS instrument do not cover the full complete column of the atmosphere however, and so the column dust optical depth value in reality is likely to be somewhere between the values derived in the polar winter during the MCS assimilation period.

Local dust storms are evident at high northern latitudes during the start of each Mars year observed by the MCS instrument, generally occurring at around $60°$N at the start of the year and steadily increasing in latitude to around $85°$N by $L_S = 90°$. These local dust storms have also been observed by the Mars Orbiter Camera and Mars Color Imager instruments (Cantor et al., 2010) on the same spacecraft as TES and MCS respectively. Local dust storms during the TES period at high northern latitudes after northern polar winter are likely to be obscured initially in the OpenMARS reanalysis by the visible column dust optical depth values carried through northern polar winter that correspond to the last available TES retrieval at the beginning of polar winter.

4. A comparison of the OpenMARS reanalysis product to assimilated observations

One method of use to indicate whether the data assimilation process has had a beneficial impact on the model output is by comparing assimilated observational data to the reanalysis and a 'control' simulation (i.e. with no data assimilation of any observations). For a successful reanalysis, the deviation of the assimilated variable from the observations assimilated should be lower in the reanalysis than when comparing the assimilated observations to a control simulation. To determine if this is the case when assimilating temperature profiles for the OpenMARS reanalysis product, a case study covering time periods of MY 28 is conducted. A time period covering the assimilation of MCS data is chosen since the MCS temperature profiles extend to a greater altitude than TES temperature profiles. Mars Year 28 is chosen as it covers a period in which a large number of MCS temperature profiles are assimilated, in particular around aphelion (see Fig. 3). Also, the TES temperature profiles have previously been compared to a similar reanalysis dataset in Lewis et al. (2007), the TES water vapour retrievals have been compared to a similar reanalysis dataset in Steele et al. (2014b) and the SPICAM ozone retrievals have been investigated in Holmes et al. (2018).

A comparison of the 3 p.m. zonal-mean atmospheric temperature at different pressure levels averaged over $L_S = 120$–$150°$ MY 28 in a control simulation and OpenMARS reanalysis dataset with MCS daytime retrievals is shown in Fig. 10. The comparison of the MCS temperature retrievals with the OpenMARS reanalysis dataset and control simulation is not exactly direct because the MCS tmperature retrievals used for the comparison range in local time from 9 a.m. to 9 p.m., although the majority of MCS temperature retrievals will have local times close to 3 p.m. Below 100 Pa, a control simulation can be up to 10 K cooler than the MCS
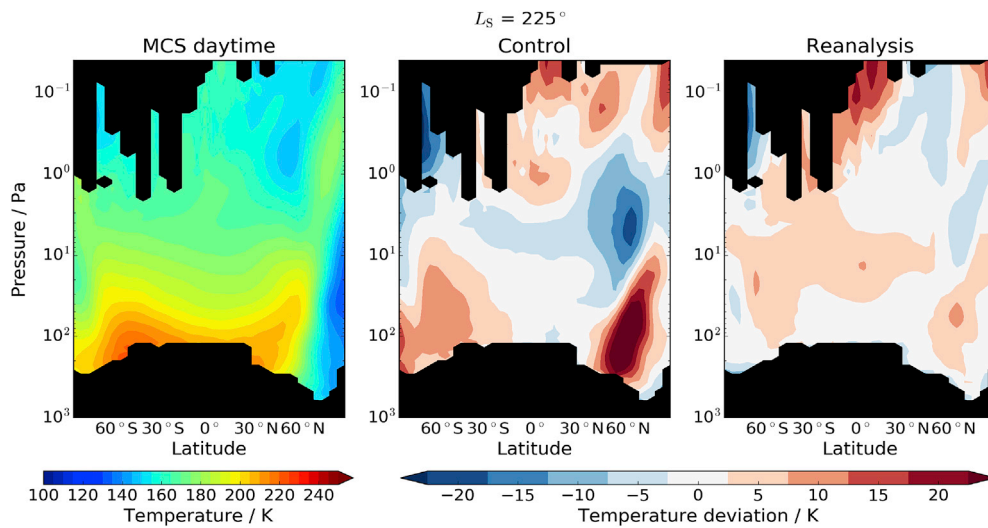
Fig. 11. Latitude-altitude plots of zonally and temporally averaged MCS daytime temperature retrievals (left), MCS–control temperature deviations (middle) and MCS–reanalysis temperature deviations (right). The temperature and temperature deviation are temporally averaged over a 30° L_S time period centred on $L_S = 225°$ MY 28. Black indicates regions of no data.
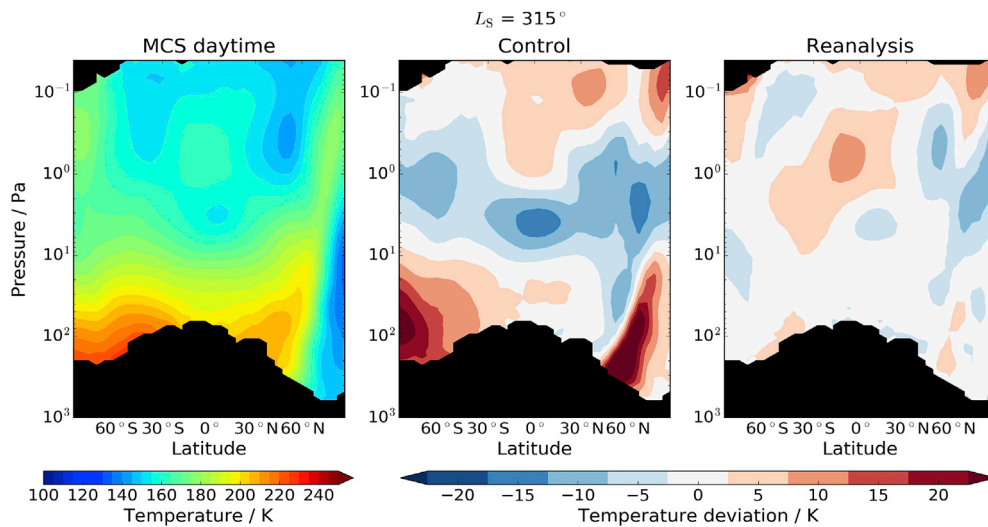

Fig. 12. Latitude-altitude plots of zonally and temporally averaged MCS daytime temperature retrievals (left), MCS–control temperature deviations (middle) and MCS–reanalysis temperature deviations (right). The temperature and temperature deviation are temporally averaged over a 30° L_S time period centred on $L_S = 315°$ MY 28. Black indicates regions of no data.

temperature retrievals, while the OpenMARS reanalysis dataset is primarily within ±5 K of the MCS temperature retrievals. In the middle atmosphere (i.e. from 100 to 1 Pa), a control simulation displays a global warm bias, with the largest warm bias of greater than 20 K peaking at around 60°S at 10 Pa. In the OpenMARS reanalysis dataset, the middle atmosphere warm bias is greatly reduced, with a factor of two reduction in the largest middle atmosphere temperature bias identified in a control simulation.

Above 1 Pa in the atmosphere, the temperature bias in a control simulation and OpenMARS reanalysis dataset are reasonably similar although generally around 1–2 K smaller in the OpenMARS reanalysis dataset. Globally, it is clear that the temperature distribution in the OpenMARS reanalysis dataset around aphelion ($L_S = 120–150°$) displays a reduced bias when compared to a control simulation.

An identical comparison has also been performed covering the time period $L_S = 210–240°$ MY 28 and is shown in Fig. 11. During this time period, the MCS instrument retrieved more temperature profiles of the atmosphere than at any other time period covered by this instrument (see

Fig. 3). The increased dust in the atmosphere did however prevent the retrieval of temperature at altitudes closer to the surface, in particular in the mid-latitude region. The largest temperature bias in a control simulation, when compared to the MCS retrievals of temperature, is a cold bias greater than 20 K centred at 60°N and 100 Pa. As seen in the previous time period investigated (Fig. 10), the OpenMARS reanalysis dataset greatly reduces the cold bias by a factor of at least two. A weaker cold bias of just over 5 K is present over the southern polar region in a control simulation below 10 Pa, which is reduced to around ±5 K in the OpenMARS reanalysis dataset.

The polar warming over the northern polar region from 10 to 1 Pa is up to 20 K too warm in a control simulation, but is well captured in the OpenMARS reanalysis dataset. The OpenMARS reanalysis dataset again displays temperature biases of at most around ±5 K for the majority of the atmosphere, with the largest temperature bias present above 0.1 Pa over the equator.

The final time period used for the investigation of temperature biases when comparing the OpenMARS reanalysis dataset and a control simu-

Table 1
Dimensions used for variables in the OpenMARS reanalysis data files.

Dimension	Number of values	Description
lon	72	Longitude
lat	36	Latitude
lev	35	Vertical level
time	360 [240]	Time

Table 2
One-dimensional variables contained in the OpenMARS reanalysis data files.

Variable	Dimension	Description	Units
lon	lon	Longitude	Degrees east
lat	lat	Latitude	Degrees north
lev	lev	Model sigma level	NU
time	time	Martian Sol	Sols since 0.0
Ls	time	Solar longitude	Degrees
MY	time	Mars Year	NU

Table 3
Surface variables contained in the OpenMARS MY 24–27 and MY 28–32 standard reanalysis data files.

Variable	Dimension	Description	Units
ps	lon, lat, time	Surface pressure	Pa
tsurf	lon, lat, time	Surface temperature	K
co2ice	lon, lat, time	Surface CO_2 ice	kg/m^2

Table 4
Atmospheric variables contained in the OpenMARS MY 24–27 and MY 28–32 standard reanalysis data files.

Variable	Dimension	Description	Units
dustcol	lon, lat, time	Visible column dust optical depth	NU
temp	lon, lat, lev, time	Atmospheric temperature	K
u	lon, lat, lev, time	Zonal wind (Eastward)	m/s
v	lon, lat, lev, time	Meridional wind (Northward)	m/s

lation against MCS daytime temperature retrievals is $L_S = 300$–$330°$ MY 28 (shown in (Fig. 12). The largest temperature bias in a control simulation is again centred at around $60°$N near the surface, indicating a cold bias greater than 20 K. The weak cold bias near the surface at southern polar latitudes during $L_S = 210$–$240°$ (Fig. 11) has strengthened by $L_S = 300$–$330°$ to match the strong cold bias at $60°$N. Both of these large biases are non-existent in the OpenMARS reanalysis dataset, which deviates from the MCS daytime retrievals by less than 5 K in the same regions. A warm temperature bias of up to around 15 K across all latitudes at around 1 Pa in a control simulation is also reduced in the OpenMARS reanalysis dataset to around 5 K, with the OpenMARS reanalysis dataset more in line with the MCS temperature retrievals than a control simulation for the entirety of the atmosphere.

5. Format of the OpenMARS reanalysis product

In many respects, the format of the OpenMARS dataset is consistent with the MACDA dataset described in Montabone et al. (2014). The reanalysis produced for this dataset covers almost nine complete Mars years, with any particular data file covering 30 sols. The data files are provided in netCDF4 format which are easily accessible by common scripting software such as Python (a sample python script for accessing the dataset is included in the dataset repository). The OpenMARS reanalysis product is split into four separate datasets: the MY 24–27 standard database (covering the TES time period of $L_S = 98°$ MY 24 to $L_S = 86°$ MY 27), MY 28–32 standard database (covering the MCS time period of $L_S = 109°$ MY 28 to $L_S = 351°$ MY 32), a water vapour column database (covering $L_S = 173°$ MY 24 to $L_S = 186°$ MY 25) and a ozone column database (covering $L_S = 2°$ in MY 27 to $L_S = 68°$ in MY 28). All datasets apart from the MY 28–32 database are continuous in time, as a result of extended gaps in the MCS time period when the instrument was switched off. The filename convention for the four sub datasets (the MY 24–27 and MY 28–32 standard datasets use the same convention) are as follows:

    openmars_myMM_lsL_myMM_lsL.nc
    openmars_vap_myMM_lsL_myMM_lsL.nc
    openmars_ozo_myMM_lsL_myMM_lsL.nc

Where MM (24–32) indicate the Mars Year (MY) and L_S (0–359) the start/end value of solar longitude (to the nearest integer) for each 30 sol period covered by the data file. Filenames for the water vapour column dataset and ozone column dataset are appended with vap and ozo respectively.

5.1. Dimensions

The dimensions of the reanalysis data files are listed in Table 1. The surface and atmospheric reanalysis output in the data files depend on three (longitude, latitude, time) and four dimensions (longitude, latitude, level, time) respectively, with the exceptions being the visible column dust optical depth, water vapour column and ozone column which depend on only three (longitude, latitude, time) dimensions. The horizontal grid spacing is $5°$ in both longitude and latitude, with four-dimensional atmospheric variables defined on model sigma levels σ (where $σ = p/p_s$, p is atmospheric pressure and p_s is surface pressure) that are non-dimensional terrain-following levels. There are 35 vertical levels in the OpenMARS reanalysis data product extending to an altitude of around 105 km.

The primary time variable used for each data file is the Martian sol (see Table 2 for all time variables). For ease of conversion and since the majority of the Mars science community use solar longitude and Mars year, these values are also included. The OpenMARS dataset employs the same calendar used by Montabone et al. (2014) which means there is a consistent bias of around 6 h between the model solar longitude and astronomical solar longitudes, and is therefore currently not consistent with the Mars24 algorithm (Allison, 1997).

The surface and atmospheric variables are output every 2 Martian hours starting at 2 a.m. on sol 241 of MY 24 for the MY 24–27 standard dataset, sol 2911 (sol 235 of MY 28) for the MY 28–32 standard dataset and on sol 361 of MY 24 for the water vapour column dataset, with sol 0 corresponding to $L_S = 0°$ MY 24. The ozone column dataset is output every 3 Martian hours starting at 3 a.m. on sol 2011 (sol 4 of MY 27), and hence only has 240 values of output for the time dimension.

5.2. Surface variables

The surface variables included in the OpenMARS MY 24–27 and MY 28–32 standard reanalysis data files are listed in Table 3. Although only the surface pressure is included in the reanalysis data files, the atmospheric pressure can be calculated for each vertical level of the atmosphere by multiplying the surface pressure variable ps by the corresponding sigma value of each vertical level in lev. Although none of the surface variables are directly assimilated in the OpenMARS reanalysis product, each one is altered indirectly as a result of the assimilation of temperature profiles and column dust optical depth. No surface variables are included in the water vapour column dataset (because they can be found in the MY 24–27 standard dataset of the corresponding time period) and the ozone column dataset (since no temperature retrievals were assimilated for this particular dataset).

Table 5
Atmospheric variables contained in the OpenMARS water vapour reanalysis data files.

Variable	Dimension	Description	Units
vapcol	lon, lat, time	Water vapour column abundance	kg/m^2

Table 6
Atmospheric variables contained in the OpenMARS ozone column reanalysis data files.

Variable	Dimension	Description	Units
o3col	lon, lat, time	Ozone column abundance	μm-atm

5.3. Atmospheric variables

The atmospheric variables included in the OpenMARS MY 24–27 and MY 28–32 standard reanalysis data files are listed in Table 4. As previously mentioned, as the variable dustcol is a column value it only has three dimensions whereas the other atmospheric variables are all four-dimensional. The zonal wind u and meridional wind v are positive in the eastward and northward direction respectively. Although not directly assimilated, u and v are both indirectly altered as a result of the assimilation procedure.

The atmospheric variables of temperature and dust column are not included in the final OpenMARS water vapour reanalysis product, as they can already be found in the OpenMARS MY 24–27 standard database, with only the water vapour column included in the water vapour column dataset (see Table 5).

Only atmospheric variables that were assimilated into the time period for the of SPICAM retrievals are included in the final OpenMARS ozone column reanalysis product (see Table 6). The data contained in the OpenMARS ozone column reanalysis product is identical to the assimilation investigated by Holmes et al. (2019).

6. Accessing and use of the OpenMARS reanalysis product

The OpenMars reanalysis dataset can be accessed freely through the Open Research Data Online (ORDO) repository at https://ordo.open.ac.uk/collections/OpenMARS/_database/4278950 (DOI: https://doi.org/10.21954/ou.rd.c.4278950.v1), with a sample Python script providing an example of how to access the dataset also provided in the repository along with a reference manual. The OpenMARS dataset has multiple different uses for scientists and engineers interested in Mars, such as an updated and extended investigation of transient eddies, energetics and the structure of the polar vortex. The dataset can also be used as improved boundary conditions for smaller scale studies (which generally use boundary conditions from a GCM), as expected conditions for entry, descent and landing of rovers and surface platforms on Mars and as a priori for retrievals of temperature, dust, water vapour and ozone.

Declaration of competing interest

The authors declare that they have no known competing financial interests or personal relationships that could have appeared to influence the work reported in this paper.

CRediT authorship contribution statement

James A. Holmes: Conceptualization, Methodology, Software, Validation, Formal analysis, Investigation, Data curation, Writing - original draft, Writing - review & editing. **Stephen R. Lewis:** Conceptualization, Methodology, Writing - review & editing, Supervision, Project administration, Funding acquisition. **Manish R. Patel:** Conceptualization, Methodology, Writing - review & editing, Supervision, Project administration, Funding acquisition.

Appendix A. Supplementary data

Supplementary data to this article can be found online at https://doi.org/10.1016/j.pss.2020.104962.

References

Allison, M., 1997. Accurate analytic representations of solar time and seasons on mars with applications to the pathfinder/surveyor missions. Geophys. Res. Lett. 24, 1967–1970.

Battalio, M., Szunyogh, I., Lemmon, M., 2016. Energetics of the martian atmosphere using the mars analysis correction data assimilation (MACDA) dataset. Icarus 276, 1–20.

Cantor, B.A., James, P.B., Calvin, W.M., 2010. MARCI and MOC observations of the atmosphere and surface cap in the north polar region of Mars. Icarus 208 (1), 61–81.

Colaïtis, A., Spiga, A., Hourdin, F., Rio, C., Forget, F., Millour, E., 2013. A thermal plume model for the Martian convective boundary layer. J. Geophys. Res. 118, 1468–1487.

Conrath, B.J., 1975. Thermal structure of the Martian atmosphere during the dissipation of the dust storm of 1971. Icarus 24, 36–46.

Conrath, B.J., Pearl, J.C., Smith, M.D., Maguire, W.C., Christensen, P.R., Dason, S., Kaelberer, M.S., 2000. Mars global surveyor thermal emission spectrometer (TES) observations: atmospheric temperatures during aerobraking and science phasing. J. Geophys. Res. 105 (E4), 9509–9520.

Dee, D.P., Uppala, S.M., Simmons, A.J., Berrisford, P., Poli, P., Kobayashi, S., Andrae, U., Balmaseda, M.A., Balsamo, G., Bauer, P., Bechtold, P., Beljaars, A.C.M., van de Berg, L., Bidlot, J., Bormann, N., Delsol, C., Dragani, R., Fuentes, M., Geer, A.J., Haimberger, L., Healy, S.B., Hersbach, H., Hólm, E.V., Isaksen, L., Kållberg, P., Köhler, M., Matricardi, M., McNally, A.P., Monge-Sanz, B.M., Morcrette, J.J., Park, B.K., Peubey, C., de Rosnay, P., Tavolato, C., Thépaut, J.N., Vitart, F., 2011. The ERA-Interim reanalysis: configuration and performance of the data assimilation system. Q. J. Roy. Meteorol. Soc. 137 (656), 553–597.

Forget, F., Hourdin, F., Talagrand, O., 1998. CO$_2$ Snowfall on mars: simulation with a general circulation model. Icarus 131, 302–316.

Greybush, S.J., Gillespie, H.E., Wilson, R.J., 2019a. Transient eddies in the TES/MCS ensemble mars atmosphere reanalysis system (EMARS). Icarus 317, 158–181.

Greybush, S.J., Kalnay, E., Wilson, R.J., Hoffman, R.N., Nehrkorn, T., Leidner, M., Eluszkiewicz, J., Gillespie, H.E., Wespetal, M., Zhao, Y., Hoffman, M., Dudas, P., McConnochie, T., Kleinböhl, A., Kass, D., McCleese, D., Miyoshi, T., 2019b. The ensemble mars atmosphere reanalysis system (EMARS) version 1.0. Geosci. Data J. 6, 137–150.

Greybush, S.J., Wilson, R.J., Hoffman, R.N., Hoffman, M.J., Miyoshi, T., Ide, K., McConnochie, T., Kalnay, E., 2012. Ensemble kalman filter data assimilation of thermal emission spectrometer temperature retrievals into a mars GCM. J. Geophys. Res. 117 (E11), E11008.

Heavens, N.G., Johnson, M.S., Abdou, W.A., Kass, D.M., Kleinböhl, A., McCleese, D.J., Shirley, J.H., Wilson, R.J., 2014. Seasonal and diurnal variability of detached dust layers in the tropical Martian atmosphere. J. Geophys. Res. 119 (8), 1748–1774.

Holmes, J.A., Lewis, S.R., Patel, M.R., Lefèvre, F., 2018. A reanalysis of ozone on Mars from assimilation of SPICAM observations. Icarus 302, 308–318.

Holmes, J.A., Lewis, S.R., Patel, M.R., Smith, M.D., 2019. Global analysis and forecasts of carbon monoxide on Mars. Icarus 328, 232–245.

Hunt, B.R., Kostelich, E.J., Szunyogh, I., 2007. Efficient data assimilation for spatiotemporal chaos: a local ensemble transform Kalman filter. Physica D 230 (1–2), 112–126.

Kleinböhl, A., Schofield, J.T., Kass, D.M., Abdou, W.A., Backus, C.R., Sen, B., Shirley, J.H., Lawson, W.G., Richardson, M.I., Taylor, F.W., Teanby, N.A., McCleese, D.J., 2009. Mars Climate Sounder limb profile retrieval of atmospheric temperature, pressure, and dust and water ice opacity. J. Geophys. Res. 114, 10006.

Lefèvre, F., Bertaux, J.-L., Clancy, R.T., Encrenaz, T., Fast, K., Forget, F., Lebonnois, S., Montmessin, F., Perrier, S., 2008. Heterogeneous chemistry in the atmosphere of Mars. Nature 454, 971–975.

Lefèvre, F., Lebonnois, S., Montmessin, F., Forget, F., 2004. Three-dimensional modeling of ozone on Mars. J. Geophys. Res. 109, E07004.

Lewis, S.R., Barker, P.R., 2005. Atmospheric tides in a Mars general circulation model with data assimilation. Adv. Space Res. 36, 2162–2168.

Lewis, S.R., Collins, M., Read, P.L., 1997. Data assimilation with a martian atmospheric GCM: an example using thermal data. Adv. Space Res. 19, 1267–1270.

Lewis, S.R., Collins, M., Read, P.L., Forget, F., Hourdin, F., Fournier, R., Hourdin, C., Talagrand, O., Huot, J.-P., 1999. A climate database for Mars. J. Geophys. Res. 104 (E10), 24177–24194.

Lewis, S.R., Read, P.L., Collins, M., 1996. Martian atmospheric data assimilation with a simplified general circulation model: orbiter and lander networks. Planet. Space Sci. 44, 1395–1409.

Lewis, S.R., Read, P.L., Conrath, B.J., Pearl, J.C., Smith, M.D., 2007. Assimilation of thermal emission spectrometer atmospheric data during the Mars Global Surveyor aerobraking period. Icarus 192, 327–347.

Lorenc, A.C., Bell, R.S., MacPherson, B., 1991. The Meteorological Office analysis correction data assimilation scheme. Q. J. Roy. Meteorol. Soc. 117, 59–89.

Madeleine, J.-B., Forget, F., Millour, E., Montabone, L., Wolff, M.J., 2011. Revisiting the radiative impact of dust on mars using the LMD global climate model. J. Geophys. Res. 116, 11010.

Madeleine, J.B., Forget, F., Millour, E., Navarro, T., Spiga, A., 2012. The influence of radiatively active water ice clouds on the Martian climate. Geophys. Res. Lett. 39 (23), L23202.

McCleese, D.J., Schofield, J.T., Taylor, F.W., Calcutt, S.B., Foote, M.C., Kass, D.M., Leovy, C.B., Paige, D.A., Read, P.L., Zurek, R.W., 2007. Mars Climate Sounder: an investigation of thermal and water vapor structure, dust and condensate distributions in the atmosphere, and energy balance of the polar regions. J. Geophys. Res. 112, 5.

Montabone, L., Forget, F., Millour, E., Wilson, R.J., Lewis, S.R., Cantor, B., Kass, D., Kleinboehl, A., Lemmon, M., Smith, M.D., Wolff, M.J., 2015. Eight-year climatology of dust optical depth on mars. Icarus 251, 65–95.

Montabone, L., Lewis, S.R., Read, P.L., 2005. Interannual variability of Martian dust storms in assimilation of several years of Mars global surveyor observations. Adv. Space Res. 36, 2146–2155.

Montabone, L., Lewis, S.R., Read, P.L., Hinson, D.P., 2006. Validation of martian meteorological data assimilation for MGS/TES using radio occultation measurements. Icarus 185, 113–132.

Montabone, L., Marsh, K., Lewis, S.R., Read, P.L., Smith, M.D., Holmes, J., Spiga, A., Lowe, D., Pamment, A., 2014. The mars analysis correction data assimilation (MACDA) dataset V1.0. Geosci. Data J. 1 (2), 129–139.

Mooring, T.A., Wilson, R.J., 2015. Transient eddies in the MACDA Mars reanalysis. J. Geophys. Res. 120 (10), 1671–1696.

Navarro, T., Madeleine, J.-B., Forget, F., Spiga, A., Millour, E., Montmessin, F., Määttänen, A., 2014. Global climate modeling of the Martian water cycle with improved microphysics and radiatively active water ice clouds. J. Geophys. Res. 119, 1479–1495.

Newman, C.E., Lewis, S.R., Read, P.L., Forget, F., 2002. Modeling the Martian dust cycle, 1. Representations of dust transport processes. J. Geophys. Res. 107, 5123.

Perrier, S., Bertaux, J.L., Lefèvre, F., Lebonnois, S., Korablev, O., Fedorova, A., Montmessin, F., 2006. Global distribution of total ozone on Mars from SPICAM/MEX UV measurements. J. Geophys. Res. 111, E09S06.

Priestley, A., 1993. A quasi-conservative version of the semi-Lagrangian advection scheme. Mon. Weather Rev. 121, 621–629.

Smith, M.D., 2002. The annual cycle of water vapor on Mars as observed by the Thermal Emission Spectrometer. J. Geophys. Res. 107, 5115.

Smith, M.D., 2004. Interannual variability in TES atmospheric observations of Mars during 1999-2003. Icarus 167 (1), 148–165.

Smith, M.D., Pearl, J.C., Conrath, B.J., Christensen, P.R., 2000. Mars Global Surveyor Thermal Emission Spectrometer (TES) observations of dust opacity during aerobraking and science phasing. J. Geophys. Res. 105 (E4), 9539–9552.

Steele, L.J., Lewis, S.R., Patel, M.R., 2014a. The radiative impact of water ice clouds from a reanalysis of Mars Climate Sounder data. Geophys. Res. Lett. 41, 4471–4478.

Steele, L.J., Lewis, S.R., Patel, M.R., Montmessin, F., Forget, F., Smith, M.D., 2014b. The seasonal cycle of water vapour on Mars from assimilation of Thermal Emission Spectrometer data. Icarus 237, 97–115.

Waugh, D.W., Toigo, A.D., Guzewich, S.D., Greybush, S.J., Wilson, R.J., Montabone, L., 2016. Martian polar vortices: comparison of reanalyses. J. Geophys. Res. 121 (9), 1770–1785.

Wolff, M.J., Clancy, R.T., 2003. Constraints on the size of martian aerosols from thermal emission spectrometer observations. J. Geophys. Res. 108 (E9), 5097.